



Geometric Effects on Liquid Oxygen/Kerosene Bi-Swirl Injector Flow Dynamics at Supercritical Conditions

Xingjian Wang,* Yanxing Wang,† and Vigor Yang‡
Georgia Institute of Technology, Atlanta, Georgia 30332

DOI: 10.2514/1.J055952

A systematic study is carried out to investigate the flow dynamics and mixing of liquid oxygen/kerosene bi-swirl injectors at supercritical conditions. The theoretical framework is based on the full conservation laws and accommodates real fluid thermodynamics and transport theories over the entire range of fluid states. Turbulence closure is achieved using large-eddy simulation. A grid independence study was conducted to ensure appropriate numerical resolution and accurate flow physics. The liquid-film atomization and breakup processes at subcritical conditions are replaced by the turbulent mixing and diffusion processes typical at supercritical conditions. Various injector geometries, with differences in the recess region, post thickness, and kerosene annulus width, are examined to explore the influence of geometry on mixing efficiency and flow dynamics. A critical mixing line is defined to measure the mixedness of propellants. The presence of a recess region is found to advance the interaction of liquid oxygen and kerosene and improve mixing efficiency. A thicker post of the inner swirler or a wider annulus leads to a larger spreading angle of the inner liquid oxygen film and intercepts the outer kerosene film in a broader area, thereby enhancing mixing in the recess region. The flow structures in the recess region are complex, and the kerosene mass fraction decreases significantly near the post surface, which might increase the thermal load on the surface in the case of reacting flows. Appropriate selection of the post thickness, recess length, and annulus width must be carefully determined for optimum injector performance. The present study offers useful information in bi-swirl injector design and in studies of the underlying flow physics of swirl injection under supercritical conditions.

Nomenclature

h	=	post thickness
L	=	axial length of injector
l	=	recess length
p	=	pressure
p_a	=	ambient pressure
Q	=	second invariant of velocity gradient tensor
R	=	radius of discharge nozzle
$R_{in,f}$	=	radius of fuel inlet
$R_{in,o}$	=	radius of oxygen inlet
R_v	=	radius of vortex chamber
r	=	radial coordinate
T	=	temperature
U	=	velocity scale
u_x	=	axial velocity
u_θ	=	azimuthal velocity
x	=	axial coordinate
y_F	=	kerosene mass fraction
α	=	spreading angle
Δr	=	kerosene annulus width
ρ	=	density
ϕ_l	=	local equivalence ratio
ϕ_0	=	global equivalence ratio

Subscripts

a	=	ambient condition
cr	=	critical property
f	=	fuel (kerosene)
o	=	oxidizer (liquid oxygen)

I. Introduction

THIS paper focuses on the mixing characteristics and flow dynamics of a liquid–liquid bi-swirl injector, as shown schematically in Fig. 1. The model is a generic configuration representative of practical swirl injectors used in propulsion and power-generation systems [1,2], such as the RD-0110/0107 engine for the third stage of the Soyuz space vehicle and the RD-170/180 engine of the Energia and Atlas V launch vehicles. In these swirl injectors, liquid oxygen (LOX) is tangentially injected into the central part of the injector (inner swirler), while kerosene is tangentially delivered into the coaxial annulus (outer swirler). The injectors operate at pressures much higher than the critical pressures of oxygen and kerosene (see Table 1) (i.e., at supercritical conditions) [3]. A thin-LOX film flows along the wall of the inner swirler and impinges on the kerosene stream at the exit. A hollow gaseous core forms in the center region of the inner swirler, in accordance with the conservation of angular momentum. The coaxial swirl injection and ensuing flow evolution determine the combustion characteristics, in that all feedback coupling of the combustion chamber with other engine components takes place through the propellant injection process [4,5].

Swirl injector geometries have received considerable attention, and optimization of the geometry for mixing and combustion has been attempted. Existing experimental studies have focused on the effects of the LOX post recess length l (between the inner and outer swirlers) on propellant mixing behaviors [6–11]. Sasaki et al. [6] performed a cold-flow study with water and nitrogen as injectants at room conditions using direct photography. The recess region was found to narrow the spreading angle and deform the spray cone. Han et al. [8] examined the mixing characteristics of a bi-swirl injector using backlight stroboscopic photographs. Water and kerosene were used as injectants. The propellant mass distribution and mixing efficiency were found to be very sensitive to recess length. An

Presented as Paper 2016-1933 at the 54th AIAA Aerospace Sciences Meeting, San Diego, CA, 4–8 January 2016; received 24 December 2016; revision received 10 March 2017; accepted for publication 10 March 2017; published online 9 June 2017. Copyright © 2017 by the authors. Published by the American Institute of Aeronautics and Astronautics, Inc., with permission. All requests for copying and permission to reprint should be submitted to CCC at www.copyright.com; employ the ISSN 0001-1452 (print) or 1533-385X (online) to initiate your request. See also AIAA Rights and Permissions www.aiaa.org/randp.

*Postdoctoral Fellow, School of Aerospace Engineering, Member AIAA.

†Research Engineer, School of Aerospace Engineering.

‡William R. T. Oakes Professor and Chair, School of Aerospace Engineering; vigor.yang@aerospace.gatech.edu. Fellow AIAA (Corresponding Author).

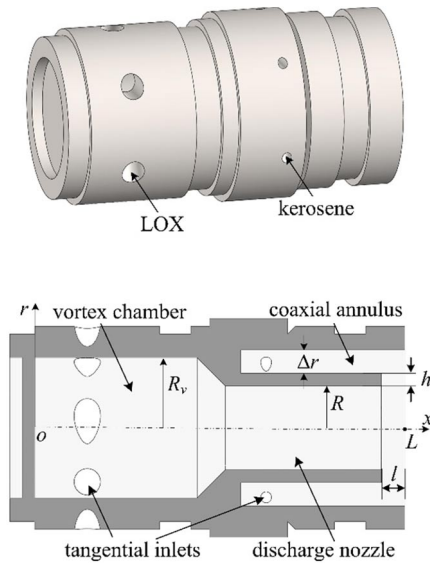


Fig. 1 Liquid-liquid bi-swirl injector.

optimum length exists to maximize the mixing efficiency. Kim et al. [12] studied the spray characteristics of water/water bi-swirl injectors. Three different mixing modes were identified: external, posttip, and internal mixing, as the recess length increases. In spite of the efforts made so far, the influence of other injector design attributes, such as the post thickness h and annulus width Δr , has yet to be explored.

Numerical simulations [13–15] have been carried out to provide more detailed information on the flow dynamics of swirl injectors, especially at supercritical conditions, where direct experimental measurement becomes extremely difficult. Zong and Yang [14] conducted a pioneering analysis of LOX swirl injectors in an axisymmetric configuration. Various hydrodynamic instabilities in the LOX film and their interactions with acoustic oscillations were identified. The effect of ambient pressure on the behavior of liquid swirl injectors was treated comprehensively by Chen and Yang [15]. Recently, Wang et al. [16] extended the axisymmetric study to include flow motion in a three-dimensional space. Special attention was paid to vorticity dynamics and circumferential flow instabilities. Volume dilation and baroclinicity were observed to play a significant role in determining the flow dynamics at supercritical conditions. The coupling between the flow instabilities in the longitudinal and azimuthal directions was investigated [17].

In spite of extensive efforts on simplex swirl injectors, very limited numerical effort has been applied to investigate bi-swirl liquid injectors, especially at supercritical pressures commonly encountered in propulsion and power-generation systems [18,19]. Heo et al. [20] examined the effects of pressure and kerosene surrogate models on LOX/kerosene mixing characteristics. The sensitivity of mixing efficiency and flow dynamics to choice of subgrid scale models was explored [21]. Wang and Yang [22,23] studied the supercritical mixing and combustion of LOX/kerosene bi-swirl injectors. The flame stabilization mechanisms were explained carefully and the kerosene annulus width was identified as an important controlling parameter. That work is considerably extended in the present study to provide more detailed insight into injector flow dynamics with different injector geometries. Numerical accuracy is first ensured by a grid independence study. The flow structures and mixing

characteristics are then discussed in depth. The effects of several injector design attributes, including the recess length, LOX post thickness, and kerosene annulus width on spreading angle and mixing efficiency are examined.

II. Theoretical and Numerical Framework

The basis of the present study is the theoretical framework described in Meng and Yang [24] and Zong et al. [25], which deals with general fluid dynamics over the entire region of thermodynamic states. The formulation is based on the full conservation laws of mass, momentum, species, and energy. Turbulence closure is achieved using the large-eddy simulation (LES) technique, in which large-scale flow motions are resolved explicitly and eddies smaller than the filter size are modeled to represent the effects of unresolved motions. Thermodynamic properties, including density, enthalpy, and specific heat at constant pressure, are evaluated according to the fundamental thermodynamics theories and a modified Soave–Redlich–Kwong equation of state [3,26,27]. Transport properties including thermal conductivity and dynamic viscosity are estimated using an extended corresponding-state principle.

Kerosene is a complex mixture of alkanes, aromatics, and cycloalkanes, and the average chemical formula for kerosene differs from one source to another. A three-component surrogate model [28], n-decane/n-propylbenzene/n-propyl-cyclohexane (74/15/11% by volume), has been shown to yield good agreement with jet-stirred reactor data and is implemented in the present study.

A self-consistent and robust numerical framework is established by implementing a preconditioning scheme and a unified treatment of general fluid thermodynamics [24]. It employs a density-based finite volume methodology, along with a dual-time-step integration technique [29]. Temporal discretization is achieved using a second-order backward difference scheme and the inner-loop pseudotime term is integrated with a four-step Runge–Kutta scheme. Spatial discretization is obtained by a fourth-order central difference scheme in generalized coordinates. The fourth-order matrix dissipation developed by Swanson and Turkel [30] is taken to ensure numerical stability and minimum contamination of the solution. Finally, a multiblock domain decomposition technique associated with the message passing interface of parallel computation is applied to optimize the numerical efficiency.

III. Injector Configuration and Flow Conditions

Figure 1 shows the liquid-liquid bi-swirl injector considered in the present study. It consists of tangential inlets, a discharge nozzle, vortex chamber, and coaxial annulus. LOX is injected tangentially into the inner swirler, while kerosene is delivered tangentially into the coaxial outer swirler. Table 2 lists the baseline geometrical parameters, where R_v , R , $R_{in,o}$, and $R_{in,f}$ denote the radii of the vortex chamber, discharge nozzle, and LOX and kerosene tangential inlets, respectively. The subscripts o and f correspond to oxidizer (oxygen) and fuel (kerosene), respectively. L , Δr , l , and h represent the injector length, the width of coaxial annulus, recess length, and post thickness, respectively. The injector operating pressure p_a and fluid states at the tangential inlets are as follows: $p_a = 10$ MPa, $T_{in,o} = 120$ K, $T_{in,f} = 300$ K, $\dot{m}_o = 0.15$ kg/s, $\dot{m}_f = 0.065$ kg/s. The injector dimensions and operating conditions are adapted from those of the RD-0110 engine; the results of the simulations will offer direct insight into the flow features of practical systems.

Table 1 Critical properties of oxygen and kerosene

Propellant	T_{cr} , K	p_{cr} , MPa	ρ_{cr} , kg/m ³
Oxygen	154.6	5.05	435.2
Kerosene	662.7	2.17	227.6

Table 2 Geometric parameters of the baseline bi-swirl injector

Parameters, mm			
R_v	R	$R_{in,o}$	$R_{in,f}$
4.5	2.7	0.85	0.35
L	l	h	Δr
24.2	1.5	0.8	0.5

The computational domain includes the injector interior ($8.4R$ in the axial direction) and a downstream region ($25R$ and $8R$ in the axial and radial directions, respectively). Because of the heavy computational effort required for calculating the flow evolution in the entire three-dimensional space, only a cylindrical section with periodic boundary conditions specified in the azimuthal direction is treated. The tangential inlets are modeled by a slit on the radial boundary of the injector. The radial and azimuthal velocities at the inlets of oxygen and kerosene are set to match the corresponding mass flow rates and swirl strength ($S = 2$). The inlet temperatures are fixed and the pressures are obtained from the radial momentum equation. The disturbances are generated by a Gaussian random-number generator with an intensity of 5% of the mean quantity and superimposed onto the mean velocity profiles to trigger turbulence. The no-slip and adiabatic boundary conditions are applied at the injector surface. At the downstream boundary, nonreflecting conditions based on the characteristic equations proposed by Li et al. [31] are applied to avoid undesirable wave reflection by extrapolation of primitive variables from the interior region. A reference pressure is applied to preserve the average pressure in the computational domain.

IV. Results and Discussion

The flow dynamics and mixing characteristics of LOX/kerosene bi-swirl injectors are systematically investigated in this section. Four cases with various geometric parameters are treated, with special attention given to the influence of recess length l , post thickness h , and annulus width Δr on injector performance. These geometric parameters play significant roles in flow mixing and stability characteristics. The present work considers four parametric cases to qualitatively examine their effects. Table 3 lists the geometric parameters for all four cases. Case 1 is the baseline, with dimensions consistent with those of the RD-0110 engine. The recess region is removed in case 2, the post thickness is enlarged in case 3, and the kerosene annulus is widened in case 4.

A. Grid Independence Study

In spite of the lack of experimental data for direct validation of the present model for bi-swirl injectors, previous studies have shown that the integrated theoretical and numerical framework employed here is capable of treating general fluids in both sub- and supercritical regimes [25,32]. To further ensure appropriate numerical accuracy, a grid independence study was performed for the baseline case, in which the recess length is 1.5 mm. Four different levels of mesh resolution were examined, as shown in Table 4. The grid size was reduced by half as the grid level increased by one. The smallest grids were located in the shear layers and wall regions to resolve steep velocity and density gradients. The Reynolds numbers of the LOX and kerosene shear layers downstream of the LOX post can be estimated as $Re_h = Uh/\nu$. The velocity scale U is taken as the

Table 3 Geometrical parameters and LOX film spreading angles of different cases

Case no.	Annulus width Δr , mm	LOX post thickness h , mm	Recess length l , mm
1 (baseline)	0.5	0.8	1.5
2	0.5	0.8	0.0
3	0.5	1.3	1.5
4	1.0	0.8	1.5

Table 4 Four levels of grid resolution

Grid level	Smallest grid size, μm	Grid points, million
1	8	0.1
2	4	0.4
3	2	1.6
4	1	6.4

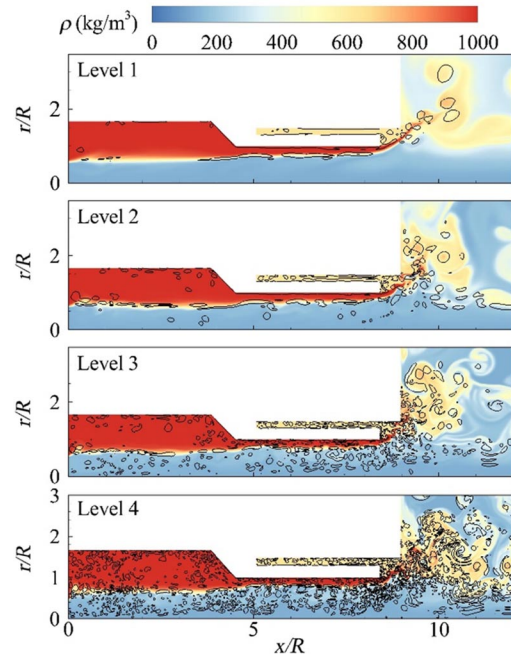


Fig. 2 Snapshots of a positive Q isocontour (solid line) at 10^8s^{-2} superimposed on the density field for increasing grid resolution.

average velocity of the LOX and kerosene streams near the post tip (i.e., 20 m/s). The kinematic viscosity ν is about $1.1 \times 10^7 \text{ m}^2/\text{s}$ for oxygen. The resultant Reynolds number is on the order of 10^5 , and the corresponding Taylor scale ($\sim \sqrt{10} h Re_h^{-1/2}$) is $8.4 \mu\text{m}$. Therefore, the level 2–4 grids provide reasonable spatial resolution within the context of LES.

Figure 2 shows snapshots of the density field with the second invariant of the velocity gradient tensor Q defined as $Q = (|\Omega|^2 - |S|^2)/2$, superimposed, to identify the vortical structures in the flowfield. Here Ω and S represent the antisymmetric and symmetric components of the velocity gradient tensor. Similarities in terms of the flow pattern, LOX film thickness, and spreading angle are observed among the four different grid levels. Small vortical structures can be captured even with the coarsest grid (level 1). As the grid resolution increases, finer vortical motions representing smaller turbulent eddies become more evident in the center gaseous core and in the LOX/kerosene mixing zone downstream of the injector exit. Further evidence [23] shows that the distributions of the mean flow properties, such as velocity components, temperature, and density, are nearly independent of the grid resolution beyond level 2. Grid level 3 was thus selected as the benchmark because of its computational efficiency and numerical accuracy.

B. Baseline Flow Dynamics

Figure 3 shows the temporal evolution of the density field for the baseline case, after the flowfield has been allowed to develop for five flowthrough times to reach a statistically stationary state (here $t = 0$ is an arbitrary moment). LOX and kerosene are tangentially introduced into the inner and outer swirlers, respectively. The flow evolution in the inner swirler is similar to that in a simplex swirler [17]. The swirl-induced centrifugal force f_c produces large pressure gradients in the radial direction ($\partial p/\partial r \sim f_c \sim \rho u_0^2/r$) and prevents the injected fluid from penetrating into the center region, leading to the generation of a gaseous core in accordance with the conservation of angular momentum. A thin liquid film forms and convects downstream along the wall. The kerosene stream fills the coaxial annulus and becomes fully developed before it reaches the LOX post tip. As the LOX film exits from the inner swirler, a spreading conical liquid sheet forms and impinges on the kerosene stream.

Figure 4 shows a close-up view of the temporal evolution of the density field near the wall of the inner swirler for the baseline case.

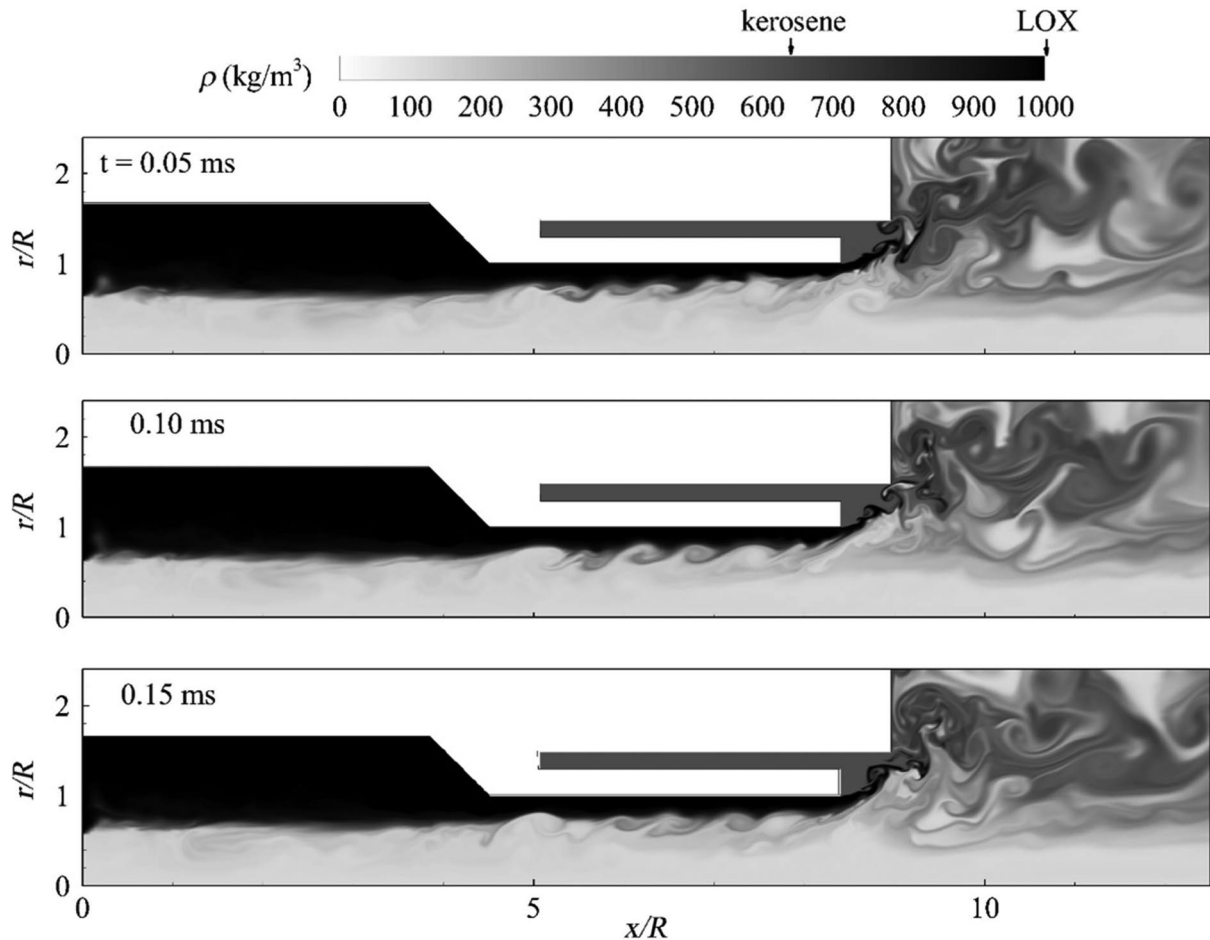


Fig. 3 Temporal evolution of the density field for the baseline (case 1).

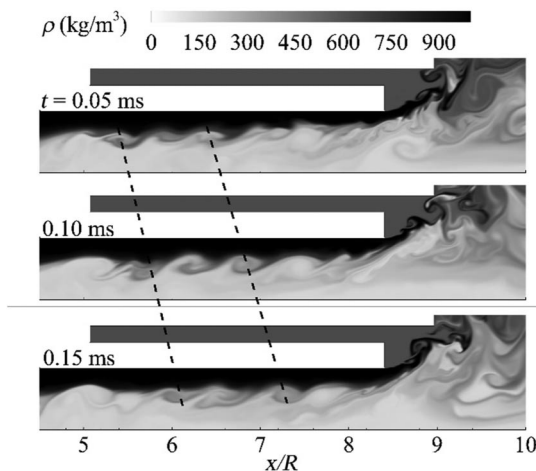


Fig. 4 Close-up view of temporal evolution of the density field near LOX film for the baseline (case 1).

The LOX film is intrinsically unstable and features hydrodynamic instabilities in both the longitudinal and circumferential directions [17], although the circumferential mode cannot be obtained in the present axisymmetric configuration. The longitudinal wave develops, grows, and travels downstream. The calculated wave speed is estimated to be 23 m/s in the discharge nozzle ($4.5 \leq x/R \leq 8.4$), following the motion of surface vortical structures with time. It agrees with the value of 25 m/s predicted by classical hydrodynamics theory [4], which regards the surface wave evolution as shallow-water wave propagation.

Figure 5 shows the instantaneous distributions of the axial and tangential velocity components and vorticity magnitude. The axial velocity of the LOX film in the vortex chamber starts from zero at the injector head end and increases substantially in the converging nozzle. This is attributed to the momentum transfer from the angular to the axial component in the converging section. The LOX film thickness in the discharge nozzle decreases in accordance with mass conservation, as shown in Fig. 3. Large vortical structures are observed in various locations, including the wall boundary layers, interfacial region between the dense liquid and light gas, and fluid mixing region. A center recirculating zone (CRZ) in the downstream region is produced with its center located at $x/R = 9.81$ and $r/R = 1.50$. A shear layer is produced in the interfacial region, where the volume dilatational and baroclinic effects heavily influence vorticity production due to steep property variations [17].

Figure 6 shows an instantaneous density field near the exit of the LOX post. Large-scale mixing between the LOX and kerosene streams is initiated in the recess region, corresponding to the internal mixing mode mentioned in Kim et al. [12]. It is noted that the momentum flux ratio of the LOX and kerosene streams is roughly 5:1 immediately downstream of the post tip. The LOX stream spreads upward, forms a conical liquid sheet, and blocks the pathway of the kerosene stream, which then adjusts its flow direction and occupies the upper part of the recess region. The LOX film surface is highly wrinkled by shear-layer instability. Traditional liquid breakup does not occur at supercritical conditions and is replaced by turbulent mixing and diffusion, through which the efficient mixing of LOX and kerosene takes place.

The interaction between the LOX and kerosene streams can be further explored by considering the injection of each fluid from its respective swirler, as shown in Fig. 7. Conical liquid sheets form for both streams. The spreading angle for the outer swirler is greater than

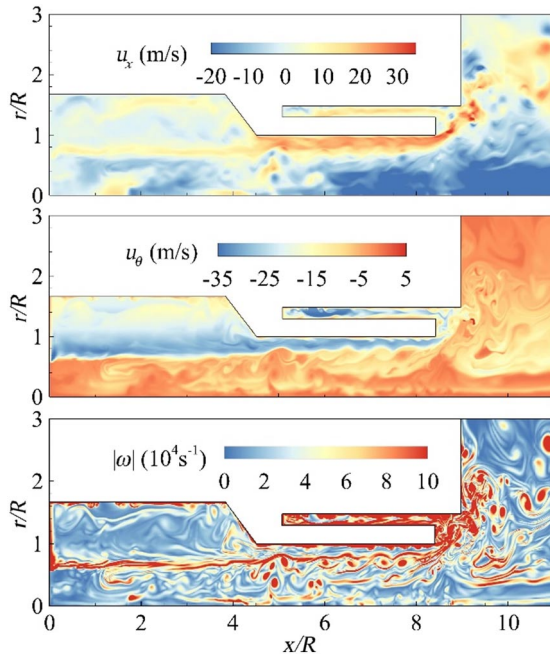


Fig. 5 Instantaneous distributions of temperature, axial velocity, and vorticity for the baseline (case 1).

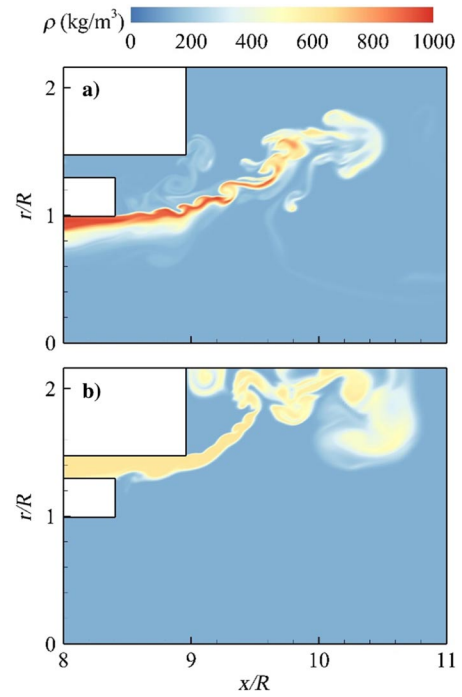


Fig. 7 Snapshots of the density field for separate injection of a) LOX only from the inner swirler and b) kerosene only from the outer swirler.

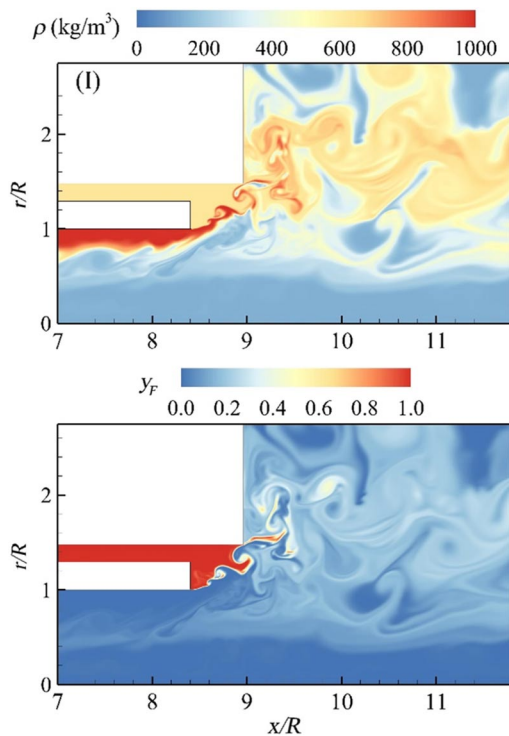


Fig. 6 Instantaneous distributions of density and kerosene mass fraction near the exit of the LOX post.

its counterpart for the inner swirler, suggesting that the two fluids would not interact if they were linearly superimposed. The situation is, however, quite different in reality, when the two fluids are injected concurrently. To elaborate, the corresponding gauge pressure ($p' = p - p_a$) fields are plotted in Fig. 8. As discussed earlier, the swirling motion induces a lower/higher pressure zone underneath/above the liquid film, respectively. The pressure drop in the recess region for the kerosene-only injection overrides the increase associated with the LOX-only injection. When both LOX and kerosene are injected, the low-pressure zone in the recess region drives the LOX stream to spread further upward, producing a larger

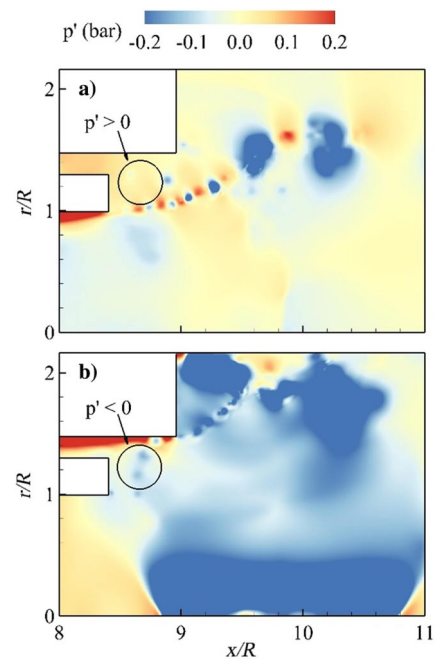


Fig. 8 Snapshots of the gauge pressure ($p - p_a$) field for separate injection of a) LOX only from the inner swirler and b) kerosene only from the outer swirler.

spreading angle. Figure 9 presents two snapshots of the density field at the initial transient and stationary stages. The spreading angle of the LOX film clearly increases in the later stage. This larger angle enables the LOX film to mix efficiently with the kerosene film in the recess region and further downstream.

C. Effects of Injector Geometry

A parametric study was performed to study the effect of injector geometry on the flow dynamics. The specific parameters are provided in Table 3.

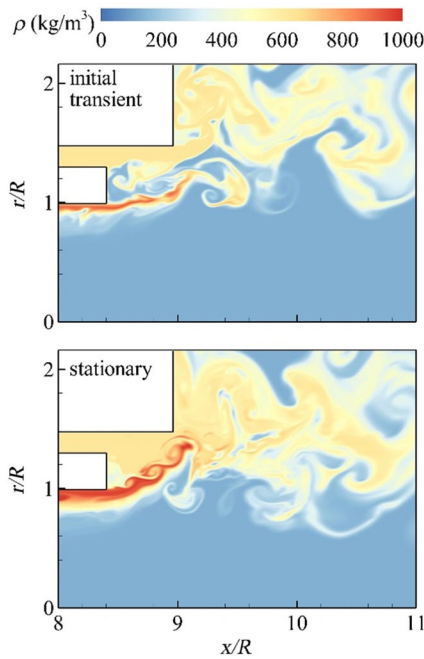


Fig. 9 Density distribution for simultaneous injection of both LOX and kerosene at two stages.

1. Recess Length (Case 2)

Figure 10 shows snapshots of the density and kerosene mass-fraction fields for the case without the recess (case 2). Several distinct features are recognizable. The absence of a recess region clearly delays propellant interaction and extends the mixing zone further downstream, undermining the mixing efficiency. The spreading angle, defined as the angle between the LOX stream and the axial direction at the injector exit, becomes smaller (30 versus 42 deg for case 1). This can be clearly observed from the time-averaged flow streamlines in Fig. 11. The CRZ becomes flatter and extends farther downstream from the injector exit than in case 1. The center is located at $x/R = 10.46$ and $r/R = 1.24$. The flow mixing in the recess region in case 1 produces two separate recirculating zones near the injector faceplate instead of one bulk bubble for case 2.

Figure 12 shows the time-averaged distributions of kerosene mass fraction for all cases in the vicinity of the injector post. Here the solid

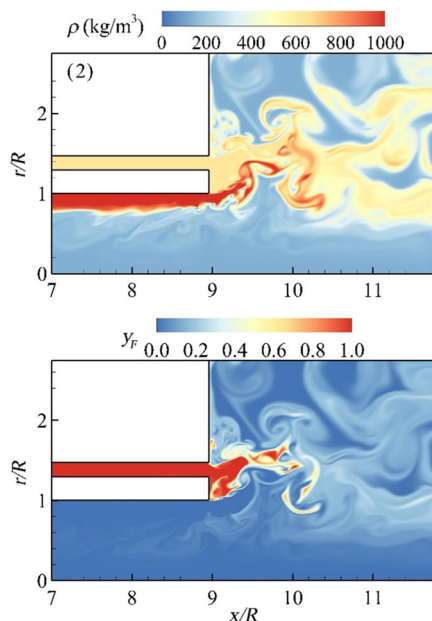


Fig. 10 Snapshots of the density and kerosene mass-fraction field for case 2 (no recess).

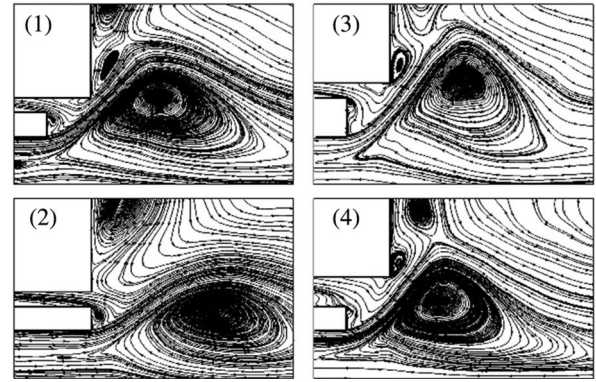


Fig. 11 Streamlines of time-averaged flowfield for all cases.

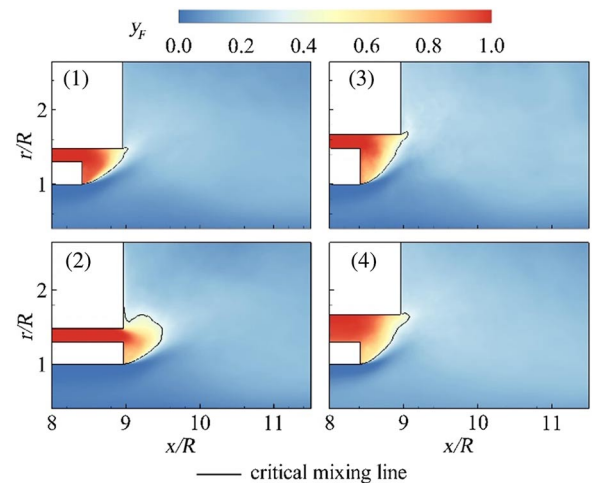


Fig. 12 Time-averaged distributions of kerosene mass fraction at injector near-field for all cases.

line is a critical mixing line, on which the local equivalence ratio ϕ_l balances the global equivalence ratio ϕ_0 (based on the inlet fuel and oxidizer mass flow rates). The difference $\phi_l - \phi_0$ measures the mixedness between kerosene and oxygen; $\phi_l - \phi_0$ is positive for the fuel-rich mixture and negative for the fuel-lean mixture. Case 1 achieves the desired mixing earlier than case 2. The kerosene mass fraction at the post surface for case 1 is higher than that for case 2. The presence of a recess region and restriction of the upper surface of the annulus forces the kerosene to flow downward instead of expanding in the chamber in case 1. The kerosene stream in case 2, however, also spreads upward in the chamber, leaving insufficient kerosene downstream of the LOX post. The recess region enhances propellant interaction and the ensuing flow dynamics, thereby improving the mixing efficiency.

2. Post Thickness (Case 3)

Figure 13 shows snapshots of the density and kerosene mass-fraction fields for case 3 with an increased post thickness ($h = 1.3$ mm). The spreading angle (56 deg) of the LOX film is higher and the center recirculation zone is steeper, as shown in Fig. 11. The larger spreading angle causes the LOX film to intercept the kerosene flow effectively over a broader area. The corresponding critical mixing line is longer, which shows that the mixing efficiency is considerably improved. The CRZ shifts slightly upward in the radial direction ($r/R = 1.72$) and downstream ($x/R = 9.88$) in the axial direction.

The LOX post in case 1 is fully covered by kerosene, which provides effective thermal protection of the post if combustion occurs. For a thicker post, however, the kerosene mass fraction near the lower portion of the LOX post is much reduced. The associated equivalence ratio is closer to the upper flammability limit, which may increase the thermal load of the post in the presence of combustion.

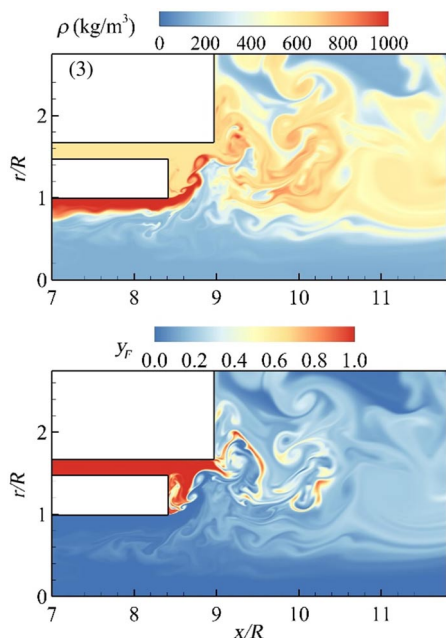


Fig. 13 Instantaneous distributions of density and kerosene mass fraction for case 3 (increased LOX post thickness).

Furthermore, the small circulation zone above the kerosene stream is closer to the injector faceplate. In the case of combustion, the hot products in this zone impose the strong heat flux on the faceplate. Future research should be conducted to determine an optimum thickness of the LOX post to achieve efficient mixing and reduced thermal loading.

3. Kerosene Annulus Width (Case 4)

Figure 14 shows the instantaneous distributions of density and kerosene mass fraction for case 4 with an increased width of the kerosene annulus ($\Delta r = 1.0$ mm). Propellant interactions become much more intensive in the recess region. The spreading angle of the LOX film increases with the annulus width and reaches 54 deg. The center of the CRZ ($x/R = 9.58$ and $r/R = 1.37$) shifts slightly upstream, and a considerable amount of the mixture downstream of the injector exit recirculates into the inner swirler. As in case 3,

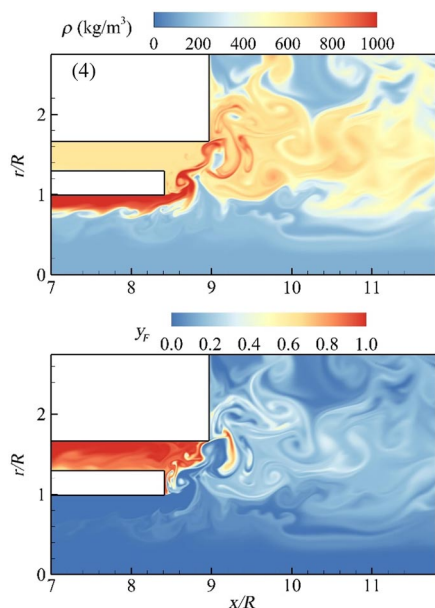


Fig. 14 Instantaneous distributions of density and kerosene mass fraction for case 4 (increased kerosene annulus width).

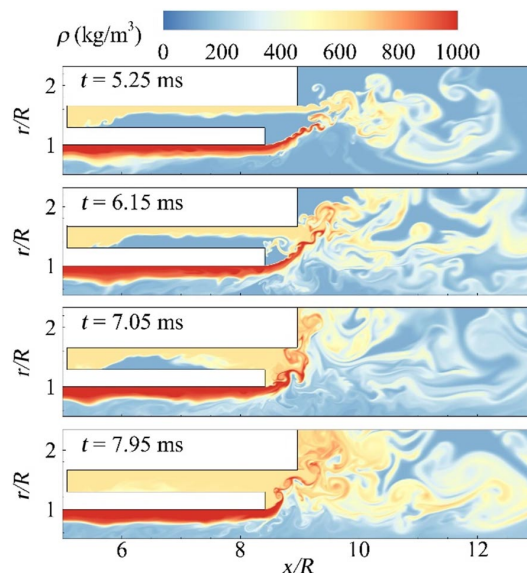


Fig. 15 Temporal evolution of the density field in the injection transient stage for case 4.

a recirculation bubble is attached to the injector faceplate and may intensify the thermal loading there.

Figure 15 shows the temporal evolution of the density field for case 4. Here $t = 0$ represents the beginning of the kerosene injection. At the initial stage of flow evolution, the thickness of the kerosene stream is smaller than the annulus width and generates a gaseous core next to the lower solid surface. The kerosene stream is then intercepted by the cone-shaped LOX spreading sheet and adjusts its flow direction. After sufficient kerosene accumulates in the recess region, it flows back into the annulus and eventually occupies the whole annulus in a fully developed state. It can be seen that a longer time is required for the kerosene stream to reach the fully developed state in the annulus (7.95 vs 5.82 ms for case 1). The complex flow structures in case 4 introduce additional shear layer in the annulus and increase momentum loss.

Figure 16 presents the radial profiles of the time-averaged density and temperature slightly upstream of the injector exit ($r/R = 8.3$). In the inner swirler, the temperature changes gradually from subcritical at the wall to supercritical in the center. A fluid transition region exists, rather than the sharp interface between a liquid and a gas occurring at subcritical pressures. Followed by this change of fluid state, the density varies smoothly from a large value in the LOX film to a small value in the gaseous core. The profiles of density and

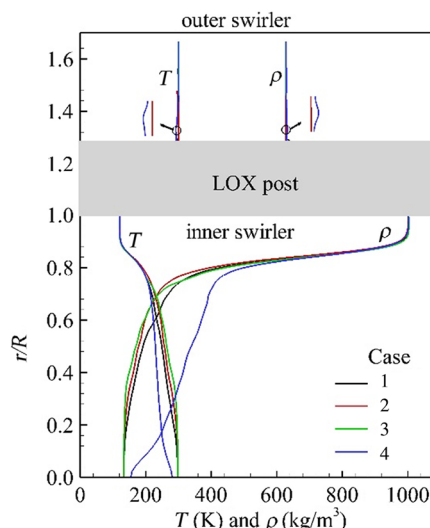


Fig. 16 Radial distributions of time-averaged density ρ and temperature T immediately upstream of the LOX post tip ($x/R = 8.3$).

Table 5 Summary of geometric effects

Case no.	Spreading angle, deg	Location of CRZ	Mixing efficiency	Post surface kerosene mass fraction
1	42	(9.81, 1.50)	— —	— —
2	30	(10.46, 1.24)	↓	↓
3	56	(9.88, 1.72)	↑	↓
4	54	(9.58, 1.37)	↑	↓

temperature near the wall ($r/R > 0.8$) are almost identical for all cases, which is consistent with the geometry of the inner swirler. Case 4 shows significant differences in the gaseous core, mainly due to the effect of the CRZ, which is closest to the LOX post and carries the kerosene fluid into the inner swirler. In the outer swirler, on the other hand, uniform distributions are observed in all cases, except that a small disturbance exists near the inner surface of the annulus in case 4. This disturbance is caused by the LOX penetration induced by large vortical structures in the recess region.

Figure 17 shows the profiles of the time-averaged axial velocity component at the same location for both inner and outer swirlers. In the inner swirler, the radial distributions of all cases are similar when $r/R > 0.5$. However, at $r/R < 0.5$, cases 1 and 4 show strong flow reversal, whereas case 3 presents a relatively weak reversal effect near the centerline. In the outer swirler, the velocity profile is nearly symmetric, with the maximum in the annulus center for cases with smaller annulus width (1–3). For case 4, the peak of the axial velocity is smaller and close to the outer surface of the annulus.

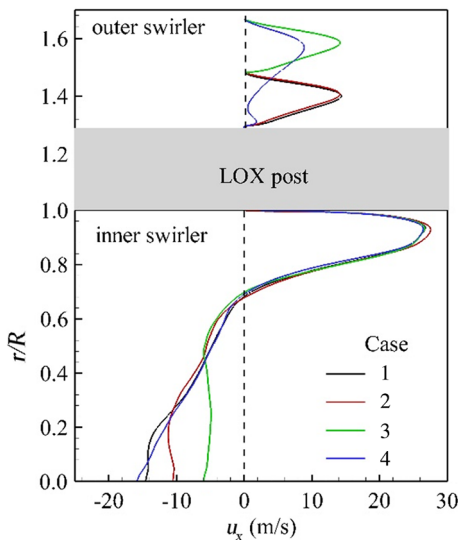


Fig. 17 Radial distributions of time-averaged axial u_x immediately upstream of the LOX post tip ($x/R = 8.3$).

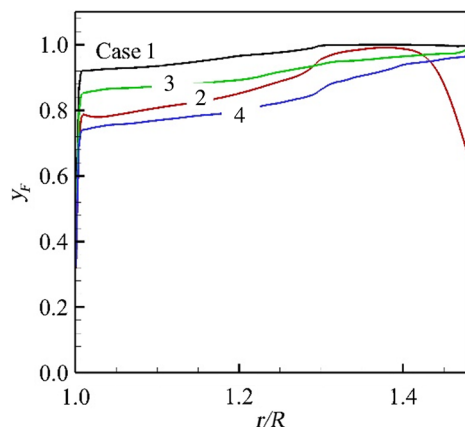


Fig. 18 Radial distribution of kerosene mass fraction at the post tip for all cases.

Figure 18 shows the radial distribution of mean kerosene mass fraction at the post surface for all cases. It is observed that the propellant mixture covering the post surface is the most kerosene rich in case 1 and the least kerosene rich in case 4, indicating that case 1 provides the best thermal protection to the post surface among the four cases. However, the spreading angle increases as either the post thickness or annulus width increases and the mixing efficiency increases accordingly. A recess region is necessary for the injector to produce a larger spreading angle and good thermal protection of the post surface.

The geometric effects are summarized in Table 5. It is noted that only two comparative cases were conducted for each geometric parameter. A more general conclusion might be obtained through further comparison of more cases in the future work. For example, a set of cases with different recess lengths could be investigated to determine an optimal length to optimize mixing and thermal protection. Similar studies could be performed on the post thickness and annulus width. In addition, it would be interesting to explore these geometric effects in reacting flows; it would also be very useful to determine whether the conclusions drawn from cold-flow studies are applicable to combustion cases.

V. Conclusions

The dynamics of LOX/kerosene bi-swirl injectors have been numerically investigated at supercritical conditions. The formulation incorporates real fluid thermodynamic properties into the conservation laws to render a unified treatment for a fluid at any thermodynamic state. Numerical accuracy was ensured by a grid independence study. The flow characteristics are discussed in detail. The flow structures in the inner swirler are similar to those of simplex swirler injectors. The low-pressure zone in the recess region induced by the kerosene stream in the outer swirler greatly increases the spreading angle of the LOX film, which intercepts the kerosene stream with a stronger momentum flux.

The effects of recess region, post thickness, and annulus width are examined in terms of mixing efficiency and flow dynamics. A critical mixing line is introduced to measure the mixedness of the propellants. The presence of a recess region is found to significantly improve mixing by advancing the interaction of propellants. The spreading angle of the LOX film increases as either the post thickness or the annulus length increases. The larger spreading angle produces a longer critical mixing line, thereby facilitating mixing. The baseline case induces the most fuel-rich mixture at the post tip surface. (This may reduce the thermal load on the post surface in combustion cases.) Although the case with an increased annulus width induces more momentum loss, it shifts the recirculation bubble upstream and recirculates the propellant mixture into the center of the injector, which could stabilize combustion in reacting flows. A more complete set of parametric studies will be required to determine the optimal configuration of recess length, post thickness, and annulus width. In the process of industrial design for real-world applications, these parameters must be selected carefully to achieve the desired injector performance.

Acknowledgements

This work was sponsored partly by the U.S. Air Force Office of Scientific Research under Grant FA 9550-10-1-0179 and partly by the William R. T. Oakes Endowment of the Georgia Institute of Technology. The authors gratefully acknowledge support and advice given by Mitat A. Birkan.

References

- [1] Rubinsky, V. R., "Instability Phenomenology and Case Studies: Combustion Instability in the RD-0110 Engine," *Liquid Rocket Engine Combustion Instability*, edited by V. Yang, and W. E. Anderson, Vol. 169, Progress in Astronautics and Aeronautics, AIAA, Washington, D.C., 1995, pp. 89–112.
doi:10.2514/5.9781600866371.0089.0112
- [2] Bazarov, V., Yang, V., and Puri, P., "Design and Dynamics of Jet and Swirl Injectors," *Liquid Rocket Thrust Chambers: Aspects of Modeling, Analysis, and Design*, edited by V. Yang, M. Habiballah, J. Hulka, and M. Popp, Vol. 200, Progress in Astronautics and Aeronautics, AIAA, Reston, VA, 2004, pp. 19–103.
doi:10.2514/4.866760
- [3] Yang, V., "Modeling of Supercritical Vaporization, Mixing, and Combustion Processes in Liquid-Fueled Propulsion Systems," *Proceedings of the Combustion Institute*, Vol. 28, No. 1, 2000, pp. 925–942.
doi:10.1016/S0082-0784(00)80299-4
- [4] Bazarov, V. G., and Yang, V., "Liquid-Propellant Rocket Engine Injector Dynamics," *Journal of Propulsion and Power*, Vol. 14, No. 5, 1998, pp. 797–806.
doi:10.2514/2.5343
- [5] Ahn, K., and Choi, H.-S., "Combustion Dynamics of Swirl Coaxial Injectors in Fuel-Rich Combustion," *Journal of Propulsion and Power*, Vol. 28, No. 6, 2012, pp. 1359–1367.
doi:10.2514/1.B34448
- [6] Sasaki, M., Sakamoto, H., Takahashi, M., Tomita, T., and Tamura, H. N., "Comparative Study of Recessed and Non-Recessed Swirl Coaxial Injectors," AIAA Paper 1997-2907, 1997.
doi:10.2514/6.1997-2907
- [7] Inamura, T., Tamura, H., and Sakamoto, H., "Characteristics of Liquid Film and Spray Injected from Swirl Coaxial Injector," *Journal of Propulsion and Power*, Vol. 19, No. 4, 2003, pp. 632–639.
doi:10.2514/2.6151
- [8] Han, P.-G., Seol, J., Hwang, S., and Yoon, Y., "The Spray Characteristics of Swirl Coaxial Injectors," AIAA Paper 2003-490, 2003.
- [9] Yang, L.-J., Ge, M.-H., Zhang, M.-Z., Fu, Q.-F., and Cai, G.-B., "Spray Characteristics of Recessed Gas-Liquid Coaxial Swirl Injector," *Journal of Propulsion and Power*, Vol. 24, No. 6, 2008, pp. 1332–1339.
doi:10.2514/1.23977
- [10] Im, J.-H., Cho, S., Yoon, Y., and Moon, I., "Comparative Study of Spray Characteristics of Gas-Centered and Liquid-Centered Swirl Coaxial Injectors," *Journal of Propulsion and Power*, Vol. 26, No. 6, 2010, pp. 1196–1204.
doi:10.2514/1.48436
- [11] Kang, Z., Li, Q., Cheng, P., Zhang, X., and Wang, Z., "Effects of Recess on the Self-Pulsation Characteristics of Liquid-Centered Swirl Coaxial Injectors," *Journal of Propulsion and Power*, Vol. 32, No. 5, 2016, pp. 1124–1132.
doi:10.2514/1.B35632
- [12] Kim, D., Han, P., Im, J.-H., Yoon, Y., and Bazarov, V. G., "Effect of Recess on the Spray Characteristics of Liquid-Liquid Swirl Coaxial Injectors," *Journal of Propulsion and Power*, Vol. 23, No. 6, 2007, pp. 1194–1203.
doi:10.2514/1.30450
- [13] Fu, Q.-F., Yang, L.-J., Qu, Y.-Y., and Gu, B., "Numerical Simulation of Dynamic Characteristics of an Open-End Swirl Injector," *Journal of Aerospace Power*, Vol. 9, 2010, p. 32.
- [14] Zong, N., and Yang, V., "Cryogenic Fluid Dynamics of Pressure Swirl Injectors at Supercritical Conditions," *Physics of Fluids*, Vol. 20, No. 5, 2008, Paper 056103.
doi:10.1063/1.2905287
- [15] Chen, X., and Yang, V., "Effect of Ambient Pressure on Liquid Swirl Injector Flow Dynamics," *Physics of Fluids*, Vol. 26, No. 10, 2014, Paper 102104.
doi:10.1063/1.4899261
- [16] Wang, X., Huo, H., Wang, Y., Zhang, L., and Yang, V., "A Three-Dimensional Analysis of Swirl Injector Flow Dynamics at Supercritical Conditions," AIAA Paper 2015-1827, 2015.
doi:10.2514/6.2015-1827
- [17] Wang, X., Huo, H., Wang, Y., and Yang, V., "Comprehensive Study of Cryogenic Fluid Dynamics of Swirl Injectors at Supercritical Conditions," *AIAA Journal*, 2017.
doi:10.2514/1.J055868
- [18] Yang, V., and Anderson, W., (eds.), *Liquid Rocket Engine Combustion Instability*, Vol. 169, Progress in Astronautics and Aeronautics, AIAA, Washington, D.C., 1995.
- [19] Lieuwen, T. C., and Yang, V., (eds.), *Combustion Instabilities in Gas Turbine Engines (Operational Experience, Fundamental Mechanisms and Modeling)*, Vol. 210, Progress in Astronautics and Aeronautics, AIAA, Reston, VA, 2005.
- [20] Heo, J.-Y., Kim, K.-J., Sung, H.-G., Choi, H.-S., and Yang, V., "Numerical Study on Kerosene/LOx Supercritical Mixing Characteristics of a Swirl Injector," AIAA Paper 2012-1266, 2012.
- [21] Heo, J.-Y., Hong, J.-S., and Sung, H.-G., "Effect of Dynamic SGS Model in a Kerosene-LOx Swirl Injector Under Supercritical Condition," *International Journal of Aeronautical and Space Sciences*, Vol. 16, No. 2, 2015, pp. 254–263.
doi:10.5139/IJASS.2015.16.2.254
- [22] Wang, X., and Yang, V., "Supercritical Injection and Mixing Characteristics of Liquid Oxygen/Kerosene Bi-Swirl Injectors," AIAA Paper 2016-1933, 2016.
doi:10.2514/6.2016-1933
- [23] Wang, X., and Yang, V., "Supercritical Mixing and Combustion of Liquid-Oxygen/Kerosene Bi-Swirl Injectors," *Journal of Propulsion and Power*, Vol. 33, No. 2, 2017, pp. 316–322.
doi:10.2514/1.B36262
- [24] Meng, H., and Yang, V., "A Unified Treatment of General Fluid Thermodynamics and Its Application to a Preconditioning Scheme," *Journal of Computational Physics*, Vol. 189, No. 1, 2003, pp. 277–304.
doi:10.1016/S0021-9991(03)00211-0
- [25] Zong, N., Meng, H., Hsieh, S. Y., and Yang, V., "A Numerical Study of Cryogenic Fluid Injection and Mixing Under Supercritical Conditions," *Physics of Fluids*, Vol. 16, No. 12, 2004, pp. 4248–4261.
doi:10.1063/1.1795011
- [26] Huo, H., Wang, X., and Yang, V., "A General Study of Counterflow Diffusion Flames at Subcritical and Supercritical Conditions: Oxygen/Hydrogen Mixtures," *Combustion and Flame*, Vol. 161, No. 12, 2014, pp. 3040–3050.
doi:10.1016/j.combustflame.2014.06.005
- [27] Wang, X., Huo, H., and Yang, V., "Counterflow Diffusion Flames of Oxygen and N-Alkane Hydrocarbons (CH₄-C₁₆H₃₄) at Subcritical and Supercritical Conditions," *Combustion Science and Technology*, Vol. 187, Nos. 1–2, 2014, pp. 60–82.
- [28] Dagaut, P., and Cathonnet, M., "The Ignition, Oxidation, and Combustion of Kerosene: A Review of Experimental and Kinetic Modeling," *Progress in Energy and Combustion Science*, Vol. 32, No. 1, 2006, pp. 48–92.
doi:10.1016/j.peccs.2005.10.003
- [29] Hsieh, S.-Y., and Yang, V., "A Preconditioned Flux-Differencing Scheme for Chemically Reacting Flows at All Mach Numbers," *International Journal of Computational Fluid Dynamics*, Vol. 8, No. 1, 1997, pp. 31–49.
doi:10.1080/10618569708940794
- [30] Swanson, R. C., and Turkel, E., "On Central-Difference and Upwind Schemes," *Journal of Computational Physics*, Vol. 101, No. 2, 1992, pp. 292–306.
doi:10.1016/0021-9991(92)90007-L
- [31] Li, H.-G., Zong, N., Lu, X.-Y., and Yang, V., "A Consistent Characteristic Boundary Condition for General Fluid Mixture and Its Implementation in a Preconditioning Scheme," *Advances in Applied Mathematics and Mechanics*, Vol. 4, No. 1, 2012, pp. 72–92.
doi:10.4208/aamm.11-m1160
- [32] Zong, N., and Yang, V., "Cryogenic Fluid Jets and Mixing Layers in Transcritical and Supercritical Environments," *Combustion Science and Technology*, Vol. 178, Nos. 1–3, 2006, pp. 193–227.
doi:10.1080/00102200500287613